

# Model predictive current control of surface-mounted permanent magnet synchronous motor with low torque and current ripple

Amir Masoud Bozorgi<sup>1</sup>, Mehdi Farasat<sup>1</sup>✉, Seyyedmahdi Jafarishiadeh<sup>1</sup>

<sup>1</sup>Division of Electrical and Computer engineering, Louisiana State University, Baton Rouge, LA, USA

✉ E-mail: mfarasat@lsu.edu

**Abstract:** Electromagnetic torque and stator flux of a permanent magnet synchronous motor (PMSM) can be controlled indirectly with model predictive current control (MPCC). In MPCC, a predefined cost function is minimised by selecting and applying appropriate voltage vectors to stator terminals. Since MPCC employs machine model to predict stator currents, it requires accurate knowledge of its parameters. Furthermore, MPCC results in high torque and current ripples at normal sampling rates. In this study, torque and current ripples of a surface-mounted PMSM are effectively reduced by incorporating the concept of duty cycle and applying two voltage vectors, instead of one voltage vector as in conventional MPCC, during a control period. A fuzzy logic modulator is designed and utilised to determine the duty cycles of voltage vectors. Furthermore, sensitivity of the proposed control strategy against parameter variations is alleviated by employing a full-order Luenberger observer. Various case studies are carried out on a hardware-in-the-loop setup and performance of the proposed method is compared with conventional and a recently introduced duty cycle-based predictive control. The obtained results verify the superiority of the proposed MPCC and its effectiveness in reducing the PMSM torque and current ripples with accurate and erroneous knowledge of motor parameters.

## Nomenclature

$R_s$	stator resistance
$L_d, L_q$	stator inductance ( $d$ and $q$ axes)
$\psi_f$	permanent magnet flux linkage
$u_{sd}, u_{sq}$	stator voltage ( $d$ and $q$ axes)
$i_{sd}, i_{sq}$	stator current ( $d$ and $q$ axes)
$\psi_{sd}, \psi_{sq}$	stator flux ( $d$ and $q$ axes)
$\omega_r$	electrical rotor speed
$\omega_m$	mechanical speed
$\theta$	electrical rotor angle
$p$	number of pole pairs
$T_e$	electromagnetic torque
$T_s$	sampling time
$d$	duty cycle
$i_{sd}^{\text{ref}}, i_{sq}^{\text{ref}}$	stator current reference ( $d$ and $q$ axes)
$w_d, w_q$	sum of system uncertainties ( $d$ and $q$ axes)
$\mathbf{u}$	controlled plant inputs
$n_1, n_2$	un-modelled dynamics
$\mathbf{y}$	measurements
$\mathbf{x}$	plant state variables
$e$	error of estimation
$\mathbf{A}$	state parameters matrix
$\mathbf{B}$	input parameters matrix
$\mathbf{C}$	measurement parameters matrix
$J$	MPCC cost function
$I_n$	nominal stator current
$\Delta I$	normalised stator current error
$n$	number of samples
$P_n$	motor rated power
$T_L$	load torque
$T_{\text{rip}}$	electromagnetic torque ripple

## 1 Introduction

Permanent magnet synchronous motors (PMSMs) are employed in various industrial and automotive applications thanks to features such as high torque-to-weight ratio, simple structure and reliable

performance. Field-oriented control (FOC) and direct torque control (DTC) are the two commonly used control techniques in PMSM drives. In FOC, flux and torque control are decoupled by aligning the  $d$ -axis component of the stator current with the  $d-q$  reference frame. As a result, accurate torque and flux control in steady state are achieved. Need for a coordinate transformation and accurate tuning of inner current loops are a few disadvantages of FOC. In DTC, the motor dynamics are controlled by employing a predefined switching table which accepts torque and flux errors along with flux vector phase angle as inputs, and outputs the appropriate switching state of the inverter. DTC features simple structure and fast dynamic response. However, it suffers from lack of direct control over motor currents, variable switching frequency, and high current and torque ripples. Space vector modulation (SVM)-based DTC has been proposed in the literature to address the two latter issues. Although DTC-SVM is effective in reducing the ripples and achieving constant switching frequency, it, however, adversely affects the simplicity of conventional DTC.

With the recent advancements in the digital signal processing area, model predictive control (MPC) has gained the attention of power electronics researchers and been applied to numerous converter topologies and electric drives [1–4]. Model predictive current control (MPCC) and model predictive torque control (MPTC) are conceptually similar to their classical counterpart methods, FOC and DTC, respectively. In MPTC, direct control of torque and flux is achieved by utilising a model of the system and minimising an appropriate cost function. In MPCC, a predictive, rather than proportional-integral, current loop is employed for controlling the  $d-q$  stator current components. Since MPCC provides direct control over stator currents, it is considered in this paper. However, this method suffers from high torque and current ripple, and variable switching frequency. In addition, it requires accurate knowledge of motor parameters since stator currents are predicted based on the system model, which in turn is developed from machine state equations. In order to reduce torque and current ripples, duty ratio modulation-based predictive methods are proposed in the literature. The general idea in these methods is to select and apply multiple voltage vectors (rather than one as in conventional predictive method) with fixed duty cycles (ratios). The duty cycles of voltage vectors are determined based on

achieving different optimisation goals. In [5], duty ratio of active voltage vector is determined such that the instantaneous torque is adjusted to its reference value at the end of the control period. In [6], duty cycle is determined to make the mean value of torque equal to its reference value. In [7, 8], duty ratio is calculated such that the torque ripple rms is minimised. In [9], flux and torque ripples are reduced by applying three, instead of two, voltage vectors in each control period. This method, however, is complex and offers low efficiency due to increased number of switching transitions. In [10], a new cost function, which aggregates torque and flux errors with individual weighting factors, is introduced and voltage vector duty ratios that result in reduced instantaneous, mean and rms torque error values are determined. Although these methods result in reduced torque and flux ripples, they are sensitive to motor parameter variations and computationally complex due to coordinate transformation in their structures. A simpler method is proposed in [11], where voltage vectors duty cycle is considered as the sum of absolute values of weighted torque and flux errors. Despite the simplicity of this method, the weighting factors of torque and flux errors require tuning for each operating point of the motor. In this paper, torque and current ripple is reduced by applying one active voltage vector followed by a zero vector during one control period. Fuzzy logic is employed to determine the duty ratio of active voltage vectors. The rules and inputs of the fuzzy-based modulator are designed such that the changes in motor operating point and its effect on voltage vectors duty ratios are taken into account. Compared to the existing methods, the proposed method is conceptually simple and results in significant reductions in torque and current ripples. Furthermore, sensitivity of the control system to motor parameter variations is alleviated by designing and employing a full-order Luenberger observer, with stator currents and sum of system uncertainties as state variables.

The paper is organised as follows: machine state equations, which describe the system model and are employed for predicting the stator currents, are provided in Section 2. The conventional MPCC is briefly explained in Section 3. Luenberger observer design, the proposed MPCC and fuzzy logic modulator are discussed in Section 4. Section 5 presents results of comparative studies between the proposed MPCC and conventional as well as a recently introduced duty cycle-based predictive control carried out on a hardware-in-the-loop (HIL) setup. Section 6 concludes the paper.

## 2 Machine equations

PMSM state equations are commonly expressed in the rotor synchronous reference frame since sinusoidal quantities appear as constants in steady-state condition. These equations are as follows:

$$u_{sd} = R_s i_{sd} + \frac{d\psi_{sd}}{dt} - \omega_r \psi_{sq} \quad (1)$$

$$u_{sq} = R_s i_{sq} + \frac{d\psi_{sq}}{dt} + \omega_r \psi_{sd} \quad (2)$$

$$\psi_{sd} = L_d i_{sd} + \psi_f \quad (3)$$

$$\psi_{sq} = L_q i_{sq} \quad (4)$$

$$T_e = \frac{3}{2} p (\psi_{sd} i_{sq} - \psi_{sq} i_{sd}) \quad (5)$$

Derivatives of  $d$ - and  $q$ -axis stator current components can be obtained by combining (1) and (2) with (3) and (4)

$$\frac{di_{sd}}{dt} = \frac{-R_s i_{sd} + \omega_r L_q i_{sq} + u_{sd}}{L_d} \quad (6)$$

$$\frac{di_{sq}}{dt} = \frac{-R_s i_{sq} - \omega_r L_d i_{sd} - \omega_r \psi_f + u_{sq}}{L_q} \quad (7)$$

For a surface-mounted PMSM, where  $L_d = L_q$ , (6) and (7) can be discretised as follows:

$$i_{sd}(k+1) = ai_{sd}(k) + T_s \omega_r i_{sq}(k) + bu_{sd}(k) \quad (8)$$

$$i_{sq}(k+1) = ai_{sq}(k) - T_s \omega_r i_{sd}(k) + bu_{sq}(k) + c \quad (9)$$

where

$$a = 1 - \frac{R_s T_s}{L_d}, \quad b = \frac{T_s}{L_d}, \quad c = \frac{-\omega_r \psi_f T_s}{L_d} \quad (10)$$

## 3 Conventional MPCC

MPCC is based on selecting the inverter switching states that minimise a predefined cost function, generally considered as the absolute value of error between the reference and predicted currents [12]. The stator currents can be predicted by using machine equations given in (8) and (9). In these equations,  $i_{sd}(k)$  and  $i_{sq}(k)$  are  $d$ - and  $q$ -axis components of measured stator currents at the  $k$ th sample, respectively. The voltage applied by the two-level, three-phase inverter is known at sample  $k$  as there are only eight valid switching states available. The corresponding voltage vector to each of the switching states can be substituted into (8) and (9) and subsequently, the stator currents can be predicted at the  $(k+1)$ th sample. Among the available eight switching states, the state that minimises a predefined cost function is selected and applied in the next control period. A typical cost function used in MPCC is given below:

$$J = |i_{sq}^{\text{ref}} - i_{sq}(k+1)| + |i_{sd}(k+1)| + f(i_{sd}, i_{sq}) \quad (11)$$

Here, the reference of  $d$ -axis stator current component is set to zero to achieve maximum torque per ampere (MTPA) operation. In addition,

$$f(i_{sd}, i_{sq}) = \begin{cases} 0, & \text{if } I_{\max} - \sqrt{i_{sd}^2 + i_{sq}^2} > 0 \\ Cst, & \text{otherwise} \end{cases} \quad (12)$$

$f(i_{sd}, i_{sq})$  is added to the cost function to insure that the stator currents remain within the range of inverter rated current,  $I_{\max}$ . If the stator currents exceed this limit, a constant value,  $Cst$ , which is significantly larger than the other two terms in the cost function, will be added. Hence, the switching state that results in overcurrent will not be selected.

Digital processing in real-time implementation takes the most part of each sampling period and it leads to a delay between the selected and applied voltage vectors. This issue adversely affects the tracking accuracy and performance of MPCC. In order to compensate the digital implementation delay, the state variables are predicted in the  $(k+2)$ th, rather than the  $(k+1)$ th, sample.

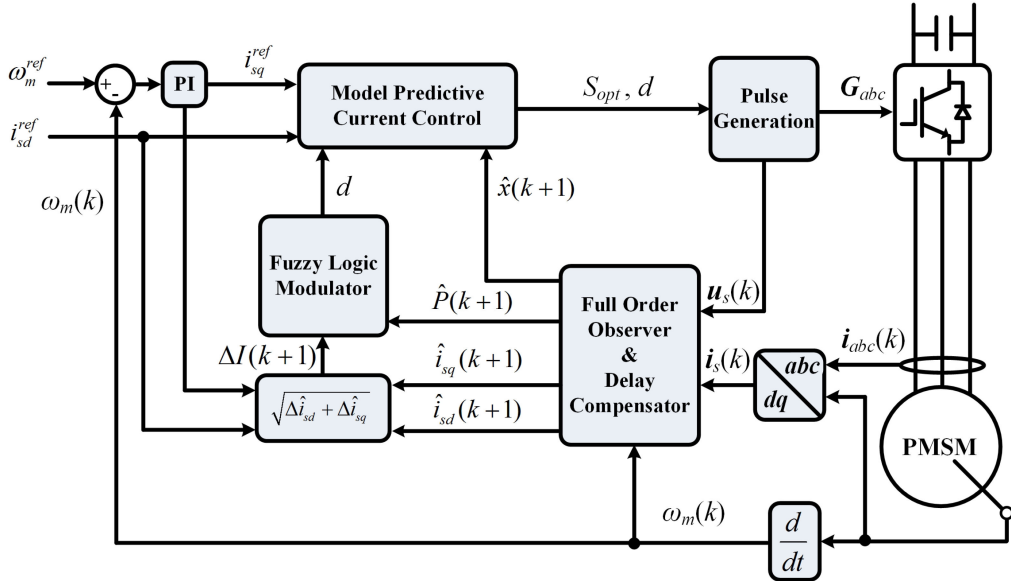
## 4 Duty cycle-based MPCC

Fig. 1 depicts the block diagram of the proposed MPCC. The  $q$ -axis stator current reference is generated by speed control section. The  $d$ -axis stator current reference is set to zero. The remaining blocks are explained in details in the following sections.

### 4.1 Luenberger observer

As mentioned earlier, performance of MPCC is degraded when system parameters are not known accurately. By introducing system parameters uncertainties in (8) and (9) as  $a = a_n + \Delta a$ ,  $b = b_n + \Delta b$ ,  $c = c_n + \Delta c$ , discretised stator current equations can be rewritten as follows:

$$i_{sd}(k+1) = a_n i_{sd}(k) + T_s \omega_r i_{sq}(k) + \frac{w_d(k)}{b_n u_{sd}(k) + (\Delta a i_{sd}(k) + \Delta b u_{sd}(k) + n_1)} \quad (13)$$



**Fig. 1** Block diagram of the proposed MPCC

$$i_{sq}(k+1) = a_n i_{sq}(k) - T_s \omega_r i_{sd}(k) + b_n u_{sq}(k) + \frac{w_q(k)}{(\Delta a i_{sq}(k) + \Delta b u_{sq}(k) + c_n + \Delta c + n_2)} \quad (14)$$

Here  $n_1$  and  $n_2$  represent the un-modelled dynamics of the system, including the machine and the inverter. Also, the errors in computation, measurement, analogue-to-digital conversion, as well as non-linear effects of modulation can be taken into account in  $n_1$  and  $n_2$ .

$w_d(k)$  and  $w_q(k)$  are dependents of changes in the system parameters such as stator resistance, inductance and flux. The rate of change of these parameters is very slow compared to system dynamics. In addition,  $i_{sdq}(k)$  and  $u_{sdq}(k)$  are dc quantities. Therefore, it can be assumed that  $w_d$  and  $w_q$  remain unchanged in two consecutive sampling instants, i.e.

$$w_d(k+1) = w_d(k) \quad (15)$$

$$w_q(k+1) = w_q(k) \quad (16)$$

By selecting  $\mathbf{x}(k) = [i_{sd}(k) \ i_{sq}(k) \ w_d(k) \ w_q(k)]^T$  as the state variable vector and  $\mathbf{u}(k) = [u_{sd}(k) \ u_{sq}(k)]^T$  as the system inputs vector, system equations in matrix form can be written as

$$\mathbf{x}(k+1) = \mathbf{A}\mathbf{x}(k) + \mathbf{B}\mathbf{u}(k) \quad (17)$$

$$\mathbf{y}(k) = \mathbf{C}\mathbf{x}(k) \quad (18)$$

In (17) and (18),  $\mathbf{A}$ ,  $\mathbf{B}$  and  $\mathbf{C}$  matrices are defined as

$$\mathbf{A} = \begin{bmatrix} a_n & T_s \omega_r & 1 & 0 \\ -T_s \omega_r & a_n & 0 & 1 \\ 0 & 0 & 1 & 0 \\ 0 & 0 & 0 & 1 \end{bmatrix} \quad (19)$$

$$\mathbf{B} = \begin{bmatrix} b_n & 0 \\ 0 & b_n \\ 0 & 0 \\ 0 & 0 \end{bmatrix} \quad (20)$$

$$\mathbf{C} = \begin{bmatrix} 1 & 0 & 0 & 0 \\ 0 & 1 & 0 & 0 \end{bmatrix}. \quad (21)$$

A full-order Luenberger observer is adopted to estimate the stator current and system parameter uncertainties. The eigenvalues of matrix  $\mathbf{A}$  are  $(L_d - R_s T_s \pm i L_d T_s \omega_r)/L_d$ . For every eigenvalue of  $\mathbf{A}$  we have

$$\text{rank} \begin{bmatrix} \mathbf{A} - \lambda \mathbf{I} \\ \mathbf{C} \end{bmatrix} = 4 \quad (22)$$

Since matrix  $\mathbf{A}$  is full rank, the system is observable.

Mathematical model of the observer based on (17) can be expressed as follows:

$$\dot{\hat{\mathbf{x}}}(k+1) = \mathbf{A}\hat{\mathbf{x}}(k) + \mathbf{B}\mathbf{u}(k) + \mathbf{G}(\mathbf{y}(k) - \hat{\mathbf{y}}(k)) \quad (23)$$

$$\hat{\mathbf{y}}(k) = \mathbf{C}\hat{\mathbf{x}}(k) \quad (24)$$

Here, variables with superscript  $\hat{\cdot}$  are estimated state variables and  $\mathbf{G}$  is the observer gain matrix. The gain should be selected in a way that the dynamic of the observer becomes faster than that of the system. In addition,  $\mathbf{G}$  should be adjusted such that the dynamic of estimation error would be asymptotically stable. The estimation error is calculated as

$$\mathbf{e}(k) = \mathbf{x}(k) - \hat{\mathbf{x}}(k) \quad (25)$$

Substituting (17) and (22) into (25), the equation of dynamic of error is obtained as

$$\begin{aligned} \mathbf{e}(k+1) &= \mathbf{x}(k+1) - \hat{\mathbf{x}}(k+1) \rightarrow \mathbf{e}(k+1) \\ &= (\mathbf{A} - \mathbf{G}\mathbf{C})\mathbf{e}(k) = \mathbf{A}_o\mathbf{e}(k) \end{aligned} \quad (26)$$

Based on (26), if the observer gain is adjusted such that the eigenvalues of matrix  $\mathbf{A}_o$  lie within the unity circle, the equation of dynamic of error would be asymptotically stable. Assuming that  $\lambda_1$ ,  $\lambda_2$ ,  $\lambda_3$  and  $\lambda_4$  are the eigenvalues of  $\mathbf{A}_o$ , matrix  $\mathbf{G}$  can be calculated from the following expression:

$$\begin{aligned} |\mathbf{I} - \mathbf{A}_o| &= |\mathbf{I} - (\mathbf{A} - \mathbf{G}\mathbf{C})| \\ &= (\lambda - \lambda_1)(\lambda - \lambda_2)(\lambda - \lambda_3)(\lambda - \lambda_4) \end{aligned} \quad (27)$$

Generally, the same dynamic is considered for  $d$ - and  $q$ -axis components, i.e.  $\lambda_1 = \lambda_2$  and  $\lambda_3 = \lambda_4$ . Following this design procedure, the estimation error approaches zero ( $\mathbf{e}(k+1) \rightarrow 0$ ) regardless of its initial value and estimated states approach their real values ( $\hat{\mathbf{x}}(k+1) \rightarrow \mathbf{x}(k+1)$ ).

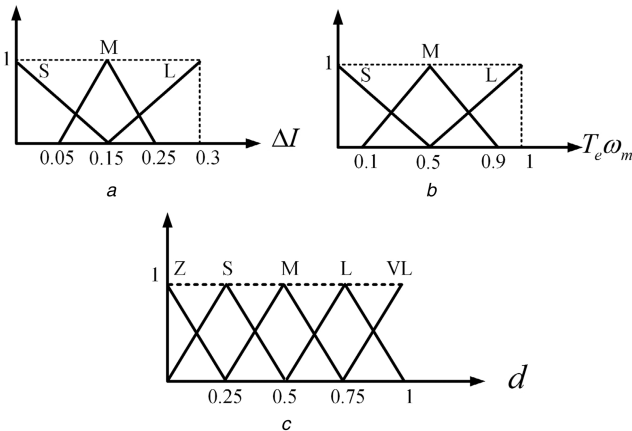


**Fig. 2** Membership distribution of fuzzy variables

(a) Stator current error, (b) Machine operating point, (c) Duty cycle

#### 4.2 Proposed MPCC

In the conventional MPCC, only one voltage vector is selected and applied to the motor during each control period. As a result, a satisfactory control performance is not achieved and significant ripples appear on the electromagnetic torque and stator currents. A simple solution to address this issue is to increase the sampling frequency. This would increase the switching transitions and limit the available time for executing control tasks, though. As an alternative, a zero voltage vector could be applied in addition to the selected active voltage vector. For this purpose, the duty ratio of the active voltage vector should be determined such that the control algorithm would satisfy a certain goal, e.g. reducing torque and current ripples. The majority of the proposed methods for determining the voltage vector duty cycle are dependent on accurate knowledge of machine parameters and also need high computational effort. In this paper, fuzzy logic algorithm is employed for determining the active voltage vector duty cycle, which will be explained in the next section.

In the proposed MPCC, after estimating the system parameter uncertainties and stator currents using the Luenburger observer and digital delay compensation,  $\hat{i}_{sq}(k+1)$  and  $\hat{i}_{sd}(k+1)$  are compared with their corresponding reference values and their errors are fed into the fuzzy logic modulator. The modulator determines duty cycle of the active switching state,  $d$ , in accordance to its inputs and fuzzy rules. The stator currents in the  $(k+2)$ th sample are then predicted as follows: (see (28))

(see (29))

Here  $a'_n$  and  $b'_n$  can be calculated by substituting  $T_s$  with  $dT_s$  in (10). Also,  $a''_n$  and  $b''_n$  can be calculated by substituting  $T_s$  with  $(1-d)T_s$  in (10).

Predicted stator currents with the available six active switching states are used to evaluate the following cost function:

$$J = \left| \hat{i}_{sq}^{\text{ref}} - \hat{i}_{sq}(k+2) \right| + \left| \hat{i}_{sd}(k+2) \right| + f(\hat{i}_{sd}(k+2), \hat{i}_{sq}(k+2)) \quad (30)$$

The active state that results in the minimum value of the cost function is selected as the next sample switching state. The selected optimum active switching state is applied for  $dT_s$  period of time

followed by a zero switching state, which is applied for  $(1-d)T_s$  period.

#### 4.3 Fuzzy-based duty cycle determination

The fuzzy logic-based modulator is designed based on Mamdani fuzzy inference system [13]. Fuzzy inference is defined as the process of mapping fuzzy logic inputs, which are crisp numerical values, to an output and consists of five steps. In the first step (fuzzification), the degree to which the inputs belong to each of fuzzy sets is determined in according to membership functions. In the second step, if a rule has more than one part, a fuzzy operator is applied to that rule and a number is generated for it. In the third step, an implication method is used to reshape the fuzzy set attributed to each rule using a function specified by the output of fuzzy operator. In the fourth step, which is known as aggregation, the reshaped functions from previous step are combined into a single fuzzy set. In this way, the effect of all rules on the output of fuzzy inference system is taken into account. In the final step, the aggregated output fuzzy set is defuzzified and a single number is generated. In this paper, minimum, maximum and maximum operators are used as fuzzy operator, implication and aggregation, respectively, and centroid criteria are employed for defuzzification.

Fuzzy logic inference inputs are defined as follows:

$$\left\{ \begin{array}{l} \text{Input 1: } \Delta I = \frac{\sqrt{(i_{sq}^{\text{ref}} - \hat{i}_{sq}(k+1))^2 + (\hat{i}_{sd}(k+1))^2}}{I_n} \\ \text{Input 2: } \hat{P}(k+1) = \frac{\hat{T}_e(k+1)\omega_m(k)}{P_n} \end{array} \right. \quad (31)$$

*Input 1* shows the discrepancy between the reference and estimated  $d$ - and  $q$ -axis stator current components, and *Input 2* reflects the dependency of duty cycle to PMSM operating point. For the sake of simplicity, just three variables are defined for each of the inputs. However, the number of variables could be increased to further enhance the accuracy of the algorithm. Membership distribution for fuzzy variables is shown in Fig. 2.

Fuzzy logic rules are summarised in Table 1. The table is designed based on the fact that for small stator current error and at partial loads, the required torque can be met by applying the active voltage vector for only a small portion of the switching period. This however changes as the current error increases or the motor operates at/close to rated load. In this case, the modulator applies the active voltage vector for longer period of time. In other words, at partial loads and for small current errors, fuzzy logic selects small duty cycles, whereas at rated load and for significant current errors, larger duty cycles are selected.

#### 5 HIL results

Various case studies are carried out on a HIL setup and performance of the proposed method is compared with conventional and a recently introduced duty cycle-based model predictive control, referred to as DRMPCC for the remainder of this paper. The setup consists of an OP4510 real-time simulator from Opal-RT Technologies Inc. operating with Kintex7 FPGA and a TI TMS320F28335 DSP. The PMSM and the feeding inverter are modelled on OP4510 with a time step of 10  $\mu$ s, while the control

$$\begin{aligned} \hat{i}_{sd}(k+1+d) &= a'_n \hat{i}_{sd}(k+1) + dT_s \omega_r(k) \hat{i}_{sq}(k+1) \\ &\quad + b'_n u_{sd}(k+1) + d\hat{w}_d(k+1) \\ \hat{i}_{sq}(k+1+d) &= a''_n \hat{i}_{sq}(k+1) - dT_s \omega_r \hat{i}_{sd}(k+1) \\ &\quad + b''_n u_{sq}(k+1) + d\hat{w}_q(k+1) \end{aligned} \quad (k+1)T_s \leq t < (k+1+d)T_s \quad (28)$$

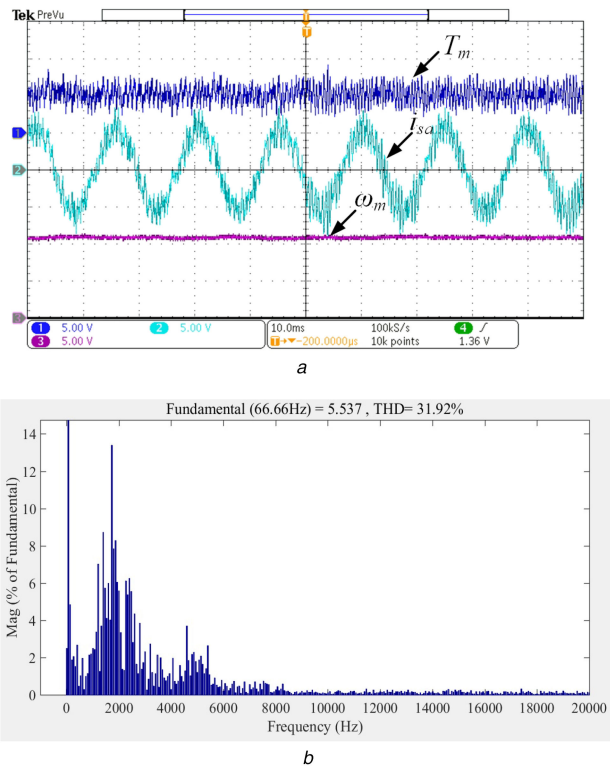
$$\begin{aligned} \hat{i}_{sd}(k+2) &= a''_n \hat{i}_{sd}(k+1+d) + (1-d)T_s \omega_r(k) \hat{i}_{sq}(k+1+d) + (1-d)\hat{w}_d(k+1) \\ \hat{i}_{sq}(k+2) &= a''_n \hat{i}_{sq}(k+1+d) - (1-d)T_s \omega_r \hat{i}_{sd}(k+1+d) + (1-d)\hat{w}_q(k+1) \end{aligned} \quad (k+1+d)T_s \leq t < (k+2)T_s \quad (29)$$

**Table 1** Fuzzy rules

Operating point	Current error		
	S	M	L
S	Z	M	L
M	S	M	L
L	L	VL	VL

**Table 2** Machine and control parameters

DC-bus voltage, V	$U_{dc}$	350
rated power, W	$P_n$	7000
rated voltage, V	$U_n$	250
rated speed, rpm	$\omega_n$	2000
pole pairs	$P$	4
rated torque, Nm	$T_n$	33
stator resistance, $\Omega$	$R_s$	0.129
inductance ( $d$ - and $q$ -axis), mH	$L_d$ and $L_q$	1.53
PM rotor flux, Wb	$\psi_f$	0.1821
sampling time, $\mu$ s	$T_s$	100
switching frequency, kHz	$f_s$	10
combined inertia, kg m <sup>2</sup>	$J$	0.003334

**Fig. 3** Steady-state response of conventional MPCC

(a) Electromagnetic torque (top, 20 Nm/div), stator phase current (middle, 16.5 A/div) and rotor mechanical speed (bottom, 477 rpm/div) under a step change in the system parameters, (b) Harmonics spectrum of stator current with erroneous system parameters

strategies are implemented on the TI DSP. Machine and control parameters are listed in Table 2. Based on these parameters and selecting  $\lambda_1 = \lambda_2 = 0.97$  and  $\lambda_3 = \lambda_4 = 0.9$ , the  $G$  and  $A_o$  matrices of the observer are calculated as

$$G = \begin{bmatrix} 0.1199 & 0.0628 \\ -0.0628 & 0.1199 \\ 0.002 & 0 \\ 0 & 0.002 \end{bmatrix}, \quad A_o = \begin{bmatrix} 0.88 & 0 & 1 & 0 \\ 0 & 0.88 & 0 & 1 \\ -0.002 & 0 & 1 & 0 \\ 0 & -0.002 & 0 & 1 \end{bmatrix} \quad (32)$$

It should be noted that the selected eigenvalues lay inside the unity circle for ensuring stability.

In DRMPCC, as proposed in [14], the stator flux and electromagnetic torque are controlled and duty cycles of switching states are calculated in a way that the developed electromagnetic torque reaches its reference value at the end of the control period. In order to carry out a fair comparison, similar approach is extended to MPCC, where the  $d$ - and  $q$ -axis components of stator current are controlled, and the following duty cycle for each switching state is obtained: (see (33)) Here  $s_{1d}$  and  $s_{1q}$  are the derivatives of  $i_{sq}$  and  $i_{sd}$  when the first voltage vector is applied and  $s_{0d}$  and  $s_{0q}$  are the derivatives of  $i_{sq}$  and  $i_{sd}$  when zero voltage vector is applied. Therefore, the stator currents can be predicted as follows:

$$i_{sd}(k+2) = i_{sd}(k+1) + dT_s s_{1d} + (1-d)T_s s_{0d} \quad (34)$$

$$i_{sq}(k+2) = i_{sq}(k+1) + dT_s s_{1q} + (1-d)T_s s_{0q} \quad (35)$$

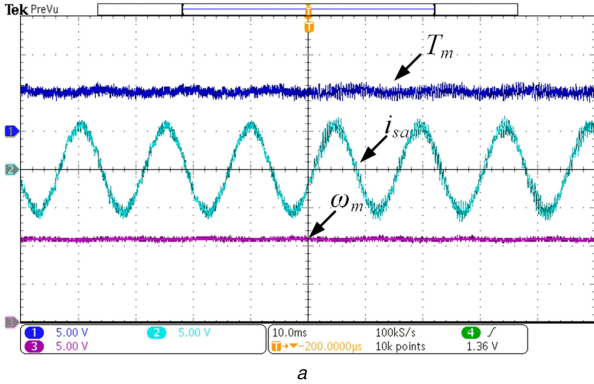
In the first scenario, the motor is operated at 1000 rpm under a load torque of 20 Nm with accurate knowledge of motor parameters for 50 ms and a step change is applied in the stator resistance and inductance values thereafter to examine the sensitivity of the three methods to parameter uncertainties. As it may happen during continuous operation of an electric motor, the stator resistance is increased by 70% and inductance is reduced by 70% of their known values. Figs. 3a–5a illustrate the motor speed, stator phase current and electromagnetic torque for conventional MPCC, DRMPCC and the proposed MPCC, respectively. Figs. 3b–5b depict the stator phase current harmonic spectrum and THD for the three methods with erroneous motor parameters. Fig. 4 illustrates the observer state variables, i.e.  $i_{sd}$ ,  $i_{sq}$ ,  $w_d$  and  $w_q$ , before and after the step change in motor parameters. It can be seen that with erroneous motor parameters,  $w_{sd}$  and  $w_{sq}$ , which are dependents of motor parameters, converge to different values (compared to their initial values), while the estimated stator currents remain almost unaffected (Figs. 6 and 7b).

The second case study compares the dynamic response of the three methods. As depicted in Figs. 5b, 6 and 7b, step changes in the reference speed, 1000–1500 rpm, and load torque, 20–25 Nm, are applied. The proposed MPCC features a slower dynamic response due to the observer. However, no significant overshoots or deviations from the reference points are observed with any of the methods (Figs. 8 and 9).

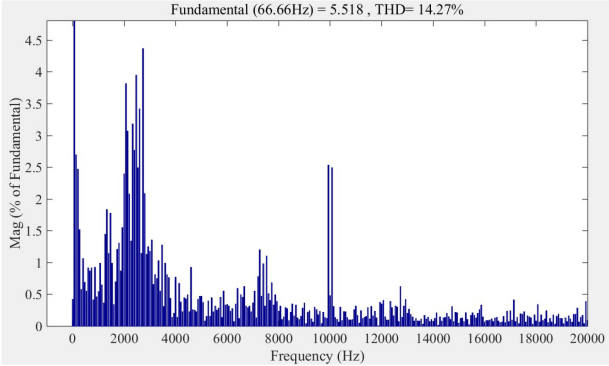
Performance of the three methods at very low speeds is evaluated as the third case study. The motor is operated at 10 rpm under a load torque of 20 Nm. Initially, the motor is controlled with accurate knowledge of parameters and after 5 s, a 70% step change in the stator resistance and inductance is applied. The motor speed, stator phase current and electromagnetic torque for conventional MPCC, DRMPCC and the proposed MPCC are shown in Figs. 10a–12a, respectively. Figs. 10b–12b depict the same waveforms for the three methods when a 100% increase is introduced in the combined rotor and load momentum of inertia.

As the last scenario, performance of the three methods with erroneous permanent magnet (PM) flux is investigated. The motor is operated at 1000 rpm under a load torque of 20 Nm. In this case study, a 70% negative error is introduced in the PM flux and the motor speed, stator phase current and electromagnetic torque waveforms under conventional MPCC, DRMPCC and the proposed MPCC are captured and illustrated in Figs. 13a–c,

$$d = \frac{(i_{sd}^{\text{ref}} - i_{sd}(k+1))(s_{1d} - s_{0d}) + (i_{sq}^{\text{ref}} - i_{sq}(k+1))(s_{1q} - s_{0q}) + T_s(s_{0d}^2 + s_{0q}^2 - s_{1d}s_{0d} - s_{1q}s_{0q})}{T_s((s_{1d} - s_{0d})^2 + (s_{1q} - s_{0q})^2)} \quad (33)$$



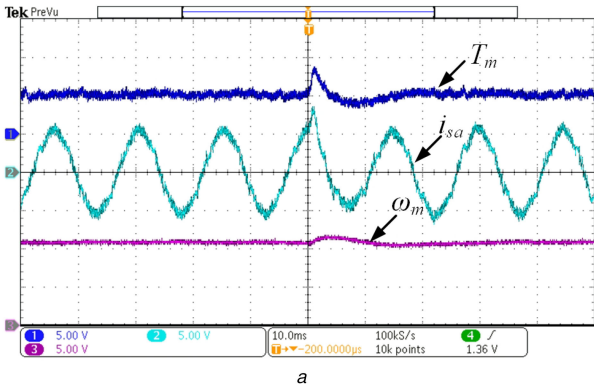
a



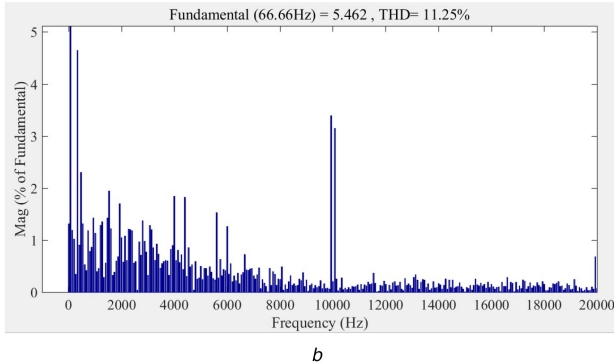
b

**Fig. 4** Steady-state response of DRMPCC

(a) Electromagnetic torque (top, 20 Nm/div), stator phase current (middle, 16.5 A/div), and rotor mechanical speed (bottom, 477 rpm/div) under a step change in the system parameters, (b) Harmonics spectrum of stator current with erroneous system parameters



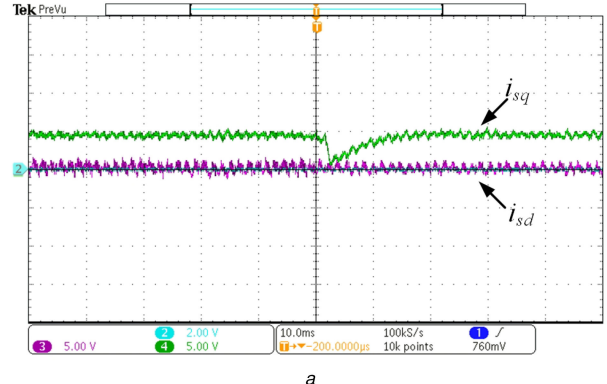
a



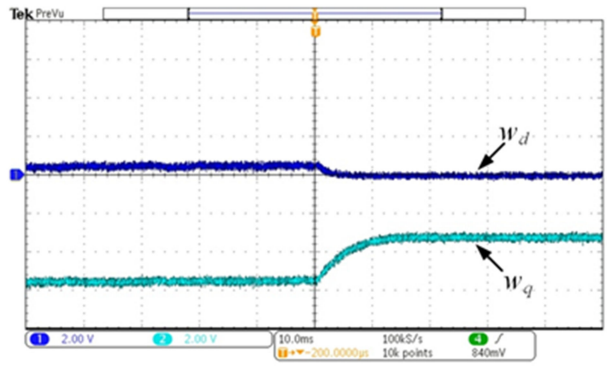
b

**Fig. 5** Steady-state response of proposed MPCC

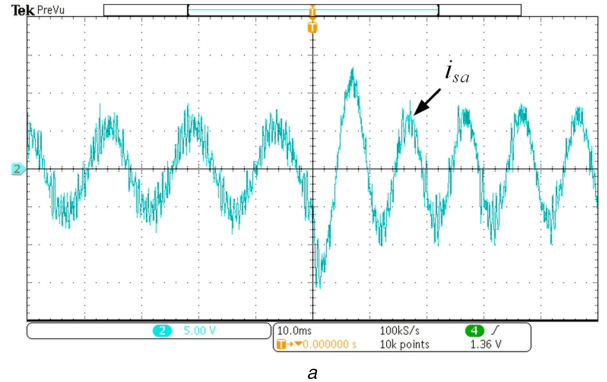
(a) Electromagnetic torque (top, 20 Nm/div), stator phase current (middle, 16.5 A/div), and rotor mechanical speed (bottom, 477 rpm/div) under a step change in the system parameters, (b) Harmonics spectrum of stator current with erroneous system parameters



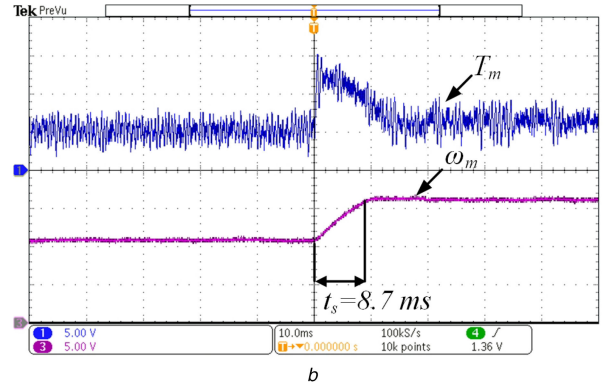
a



b

**Fig. 6** State-space variables under a step change in the system parameters  
(a) d- and q-axis components of stator current (20 A/div), (b) d- and q-axis system uncertainties (2 A/div)

a

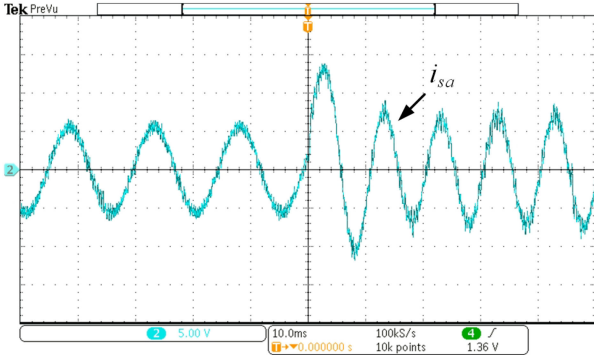


b

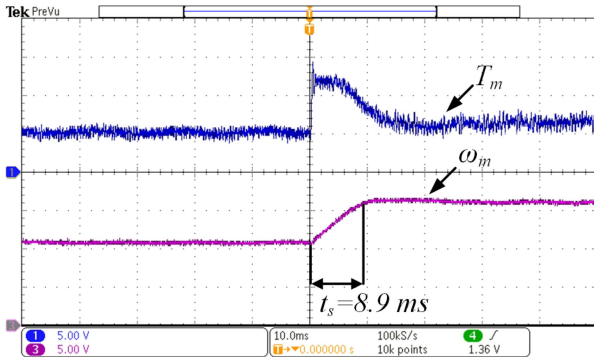
**Fig. 7** Dynamic response of conventional MPCC

(a) Stator phase current (16.5 A/div), (b) Electromagnetic torque (top, 20 Nm/div), and rotor mechanical speed (bottom, 477 rpm/div)

respectively. Since the effect of flux uncertainty is taken into account in  $w_q$ , performance of the proposed method remains almost unaffected.



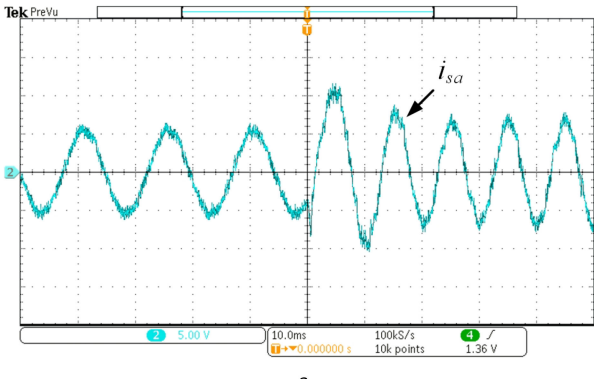
a



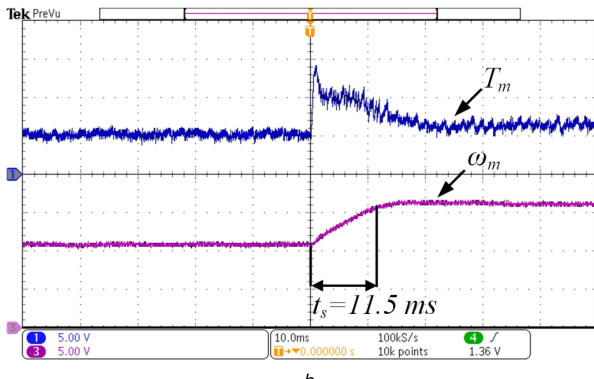
b

**Fig. 8** Dynamic response of DRMPCC

(a) Stator phase current (16.5 A/div), (b) Electromagnetic torque (top, 20 Nm/div), and rotor mechanical speed (bottom, 477 rpm/div)



a

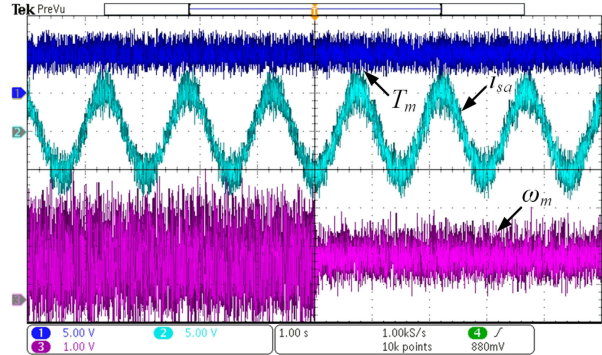


b

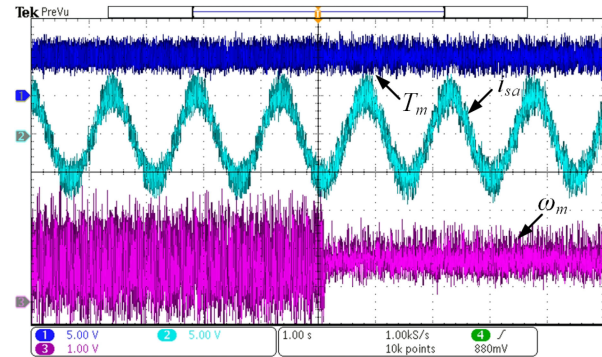
**Fig. 9** Dynamic response of proposed MPCC

(a) Stator phase current (16.5 A/div), (b) Electromagnetic torque (top, 20 Nm/div), and rotor mechanical speed (bottom, 477 rpm/div)

The stator current THD and electromagnetic torque ripple,  $T_{\text{rip}}$ , defined as in (36), for all operating conditions are summarised in Tables 3 and 4



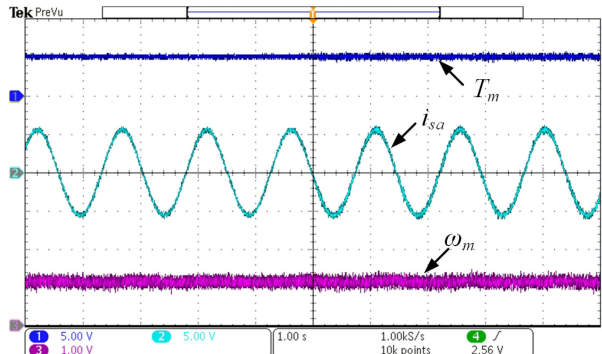
a



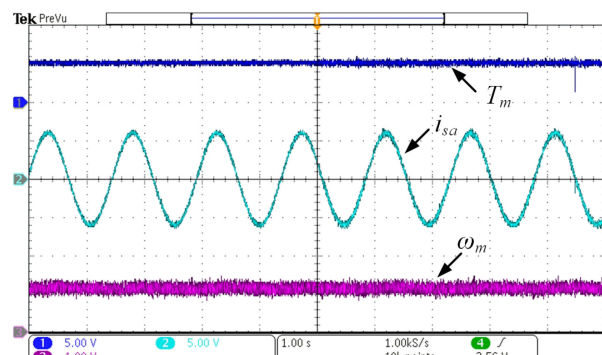
b

**Fig. 10** Electromagnetic torque (top, 20 Nm/div), stator phase current (middle, 16.5 A/div), speed (bottom, 9.5 rpm/div) under a step change in the stator resistance and inductance under conventional MPCC

(a) Normal inertia, (b) 100% increase in inertia



a

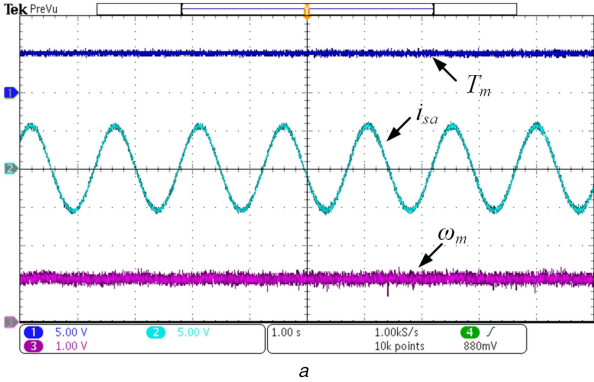


b

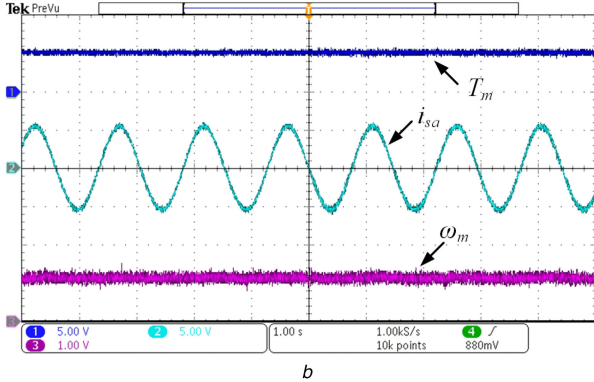
**Fig. 11** Electromagnetic torque (top, 20 Nm/div), stator phase current (middle, 16.5 A/div), speed (bottom, 9.5 rpm/div) under a step change in the stator resistance and inductance under DRMPCC

(a) Normal inertia, (b) 100% increase in inertia

$$T_{\text{rip}} = \frac{\sum_{i=1}^n |T_e(i) - T_L|}{n} \quad (36)$$



a



b

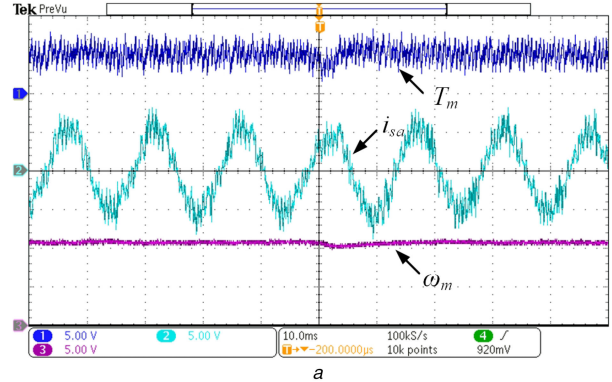
**Fig. 12** Electromagnetic torque (top, 20 Nm/div), stator phase current (middle, 16.5 A/div), speed (bottom, 9.5 rpm/div) under a step change in the stator resistance and inductance under proposed MPCC

(a) Normal inertia, (b) 100% increase in inertia

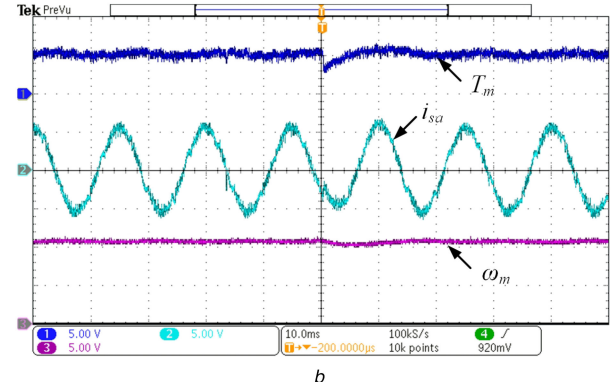
**Table 3** Stator current THD and torque ripple at high speeds

Test	Method	THD of $i_{sa}$ , %	$T_{rip}$ , Nm
$T_L = 20 \text{ Nm}, \omega_m = 1000 \text{ rpm}$ (with accurate stator parameters)	conventional MPCC	28.26	3.45
	DRMPCC	12.15	1.26
	proposed MPCC	11.02	1.22
$T_L = 20 \text{ Nm}, \omega_m = 1000 \text{ rpm}$ (with erroneous stator parameters)	conventional MPCC	31.92	3.72
	DRMPCC	14.27	1.47
	proposed MPCC	11.25	1.24
$T_L = 25 \text{ Nm}, \omega_m = 1500 \text{ rpm}$ (with erroneous stator parameters)	conventional MPCC	24.03	3.52
	DRMPCC	15.56	2.4
	proposed MPCC	11.25	1.46
$T_L = 20 \text{ Nm}, \omega_m = 1000 \text{ rpm}$ (with 70% decrease in PM flux)	conventional MPCC	27.97	3.3
	DRMPCC	11.46	1.26
	proposed MPCC	11.07	1.23

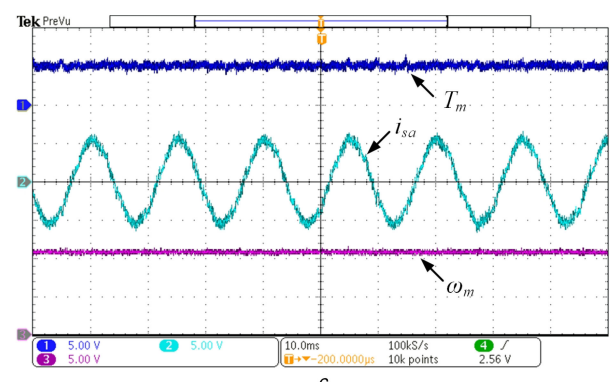
Stator current THD increases with erroneous knowledge of motor parameters when conventional MPCC and DRMPCC are employed. The proposed MPCC, however, maintains almost the same current THD in the presence of parameter uncertainties and results in significantly reduced THD in the other scenarios. The proposed MPCC outperforms its conventional counterpart in terms of torque ripple, as well. In all case studies, torque ripple is considerably lower when the motor torque and flux are (indirectly) controlled by the proposed MPCC. It is noteworthy to mention that the fuzzy rules are defined such that reductions in both



a



b



c

**Fig. 13** Electromagnetic torque (top, 20 Nm/div), stator phase current (middle, 16.5 A/div), and speed (bottom, 477 rpm/div) with a negative 70% error in PM flux

(a) Conventional MPCC, (b) DRMPCC, (c) Proposed MPCC

electromagnetic torque and stator current ripples are achieved. However, these rules could be modified in a way that reducing either torque or stator current ripples would have the priority.

## 6 Conclusion

An improved model predictive current control for surface-mounted PMSM, which results in reduced torque and stator current ripple, is introduced in this paper. Unlike conventional predictive methods, in which only one voltage vector is selected and applied during one control period, two voltage vectors are applied. The duty cycle of the active voltage vectors are determined using fuzzy logic, which is simple and does not require knowledge of machine parameters. Furthermore, a full-order Leunberger observer is designed and employed to estimate the state variables, thanks to which sensitivity of the proposed control method to system parameter variations is significantly reduced.

## 7 Acknowledgment

Research described in this paper was supported by Louisiana Board of Regents' grant no. 2015-18-RD-A-04.

**Table 4** Stator current THD and torque ripple at low speeds

Test	Method	THD of $i_{sa}$ , %	$T_{rip}$ , Nm
$T_L = 20 \text{ Nm}, \omega_m = 10 \text{ rpm}$ (with erroneous stator parameters)	conventional MPCC	29.33	4.08
	DRMPCC	6.93	0.98
	proposed MPCC	5.45	0.85
$T_L = 20 \text{ Nm}, \omega_m = 10 \text{ rpm}$ (with erroneous stator parameters and 100% increase in inertia)	conventional MPCC	26.1	3.89
	DRMPCC	6.32	1.03
	proposed MPCC	5.76	0.89
$T_L = 20 \text{ Nm}, \omega_m = 10 \text{ rpm}$ (with accurate stator parameters)	conventional MPCC	29.48	4.35
	DRMPCC	5.7	0.85
	proposed MPCC	5.51	0.81
$T_L = 20 \text{ Nm}, \omega_m = 10 \text{ rpm}$ (with accurate stator parameters and 100% increase in inertia)	conventional MPCC	27.88	4.21
	DRMPCC	5.5	0.93
	proposed MPCC	5.28	0.83

## 8 References

- [1] Liu, P., Wang, Y., Cong, W., *et al.*: ‘Grouping-sorting-optimized model predictive control for modular multilevel converter with reduced computational load’, *IEEE Trans. Power Electron.*, 2016, **31**, (3), pp. 1896–1907

- [2] Geyer, T., Quevedo, D.: ‘Performance of multistep finite control set model predictive control for power electronics’, *IEEE Trans. Power Electron.*, 2015, **30**, (3), pp. 1633–1644
- [3] Kim, S.-K., Choi, D.-K., Lee, K.-B., *et al.*: ‘Offset-free model predictive control for the power control of three-phase ac/dc converters’, *IEEE Trans. Ind. Electron.*, 2015, **62**, (11), pp. 7114–7126
- [4] Bozorgi, A., Farasat, M., Jafarishiadeh, S.: ‘Improved model predictive current control of permanent magnet synchronous machines with fuzzy based duty cycle control’. Proc. Energy Conversion Congress and Exposition (ECCE), 2016, pp. 1–6
- [5] Zhang, Y., Yang, H.: ‘Model predictive torque control of induction motor drives with optimal duty cycle control’, *IEEE Trans. Power Electron.*, 2014, **29**, (12), pp. 6593–6603
- [6] Pacas, M., Weber, J.: ‘Predictive direct torque control for the PM synchronous machine’, *IEEE Trans. Ind. Electron.*, 2005, **52**, (5), pp. 1350–1356
- [7] Kang, J., Sul, S.: ‘New direct torque control of induction motor for minimum torque ripple and constant switching frequency’, *IEEE Trans. Ind. Appl.*, 1999, **35**, (5), pp. 1076–1082
- [8] Shyu, K., Lin, J., Pham, V., *et al.*: ‘Global minimum torque ripple design for direct torque control of induction motor drives’, *IEEE Trans. Ind. Electron.*, 2010, **57**, (9), pp. 3148–3156
- [9] Zhang, Y., Zhu, J.: ‘A novel duty cycle control strategy to reduce both torque and flux ripples for DTC of permanent magnet synchronous motor drives with switching frequency reduction’, *IEEE Trans. Power Electron.*, 2011, **26**, (10), pp. 3055–3067
- [10] Niu, F., Li, K., Wang, Y.: ‘Direct torque control for permanent magnet synchronous machines based on duty ratio modulation’, *IEEE Trans. Ind. Electron.*, 2015, **62**, (10), pp. 6160–6170
- [11] Zhang, Y., Zhu, J.: ‘Direct torque control of permanent magnet synchronous motor with reduced torque ripple and commutation frequency’, *IEEE Trans. Power Electron.*, 2011, **26**, (1), pp. 235–248
- [12] Davari, S.A., Arab Khaburi, D., Wang, F., *et al.*: ‘Using full order and reduced order observers for robust sensorless predictive torque control of induction motors’, *IEEE Trans. Power Electron.*, 2012, **27**, (7), pp. 3424–3433
- [13] Romeral, L., Arias, A., Aldabas, E., *et al.*: ‘Novel direct torque control (DTC) scheme with fuzzy adaptive torque-ripple reduction’, *IEEE Trans. Ind. Electron.*, 2003, **50**, (3), pp. 487–492
- [14] Zhang, Y., Gao, S.: ‘Simultaneous optimization of voltage vector and duty cycle in model predictive torque control of PMSM drives’. Proc. 17th Int. Conf. on Electrical Machines and Systems, 2014, pp. 3338–3344